



This is a repository copy of *Comparison of periodic and free mesh on the mechanical properties prediction of 3D braided composites*.

White Rose Research Online URL for this paper:  
<http://eprints.whiterose.ac.uk/106279/>

Version: Accepted Version

---

**Article:**

Chao, Z., Curiel-Sosa, J.L. and Bui, T.Q. (2017) Comparison of periodic and free mesh on the mechanical properties prediction of 3D braided composites. *Composite Structures*, 159. pp. 667-676. ISSN 0263-8223

<https://doi.org/10.1016/j.compstruct.2016.10.012>

---

Article available under the terms of the CC-BY-NC-ND licence  
(<https://creativecommons.org/licenses/by-nc-nd/4.0/>).

**Reuse**

This article is distributed under the terms of the Creative Commons Attribution-NonCommercial-NoDerivs (CC BY-NC-ND) licence. This licence only allows you to download this work and share it with others as long as you credit the authors, but you can't change the article in any way or use it commercially. More information and the full terms of the licence here: <https://creativecommons.org/licenses/>

**Takedown**

If you consider content in White Rose Research Online to be in breach of UK law, please notify us by emailing [eprints@whiterose.ac.uk](mailto:eprints@whiterose.ac.uk) including the URL of the record and the reason for the withdrawal request.



[eprints@whiterose.ac.uk](mailto:eprints@whiterose.ac.uk)  
<https://eprints.whiterose.ac.uk/>

## Accepted Manuscript

Comparison of periodic mesh and free mesh on the mechanical properties prediction of 3D braided composites

Chao Zhang, JL Curiel-Sosa, Tinh Quoc Bui

PII: S0263-8223(16)31279-X

DOI: <http://dx.doi.org/10.1016/j.compstruct.2016.10.012>

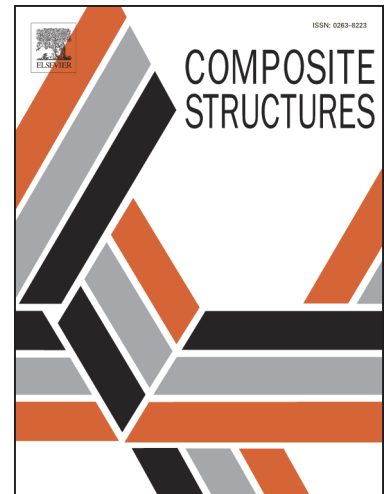
Reference: COST 7838

To appear in: *Composite Structures*

Received Date: 21 July 2016

Revised Date: 4 October 2016

Accepted Date: 6 October 2016



Please cite this article as: Zhang, C., Curiel-Sosa, J., Bui, T.Q., Comparison of periodic mesh and free mesh on the mechanical properties prediction of 3D braided composites, *Composite Structures* (2016), doi: <http://dx.doi.org/10.1016/j.compstruct.2016.10.012>

This is a PDF file of an unedited manuscript that has been accepted for publication. As a service to our customers we are providing this early version of the manuscript. The manuscript will undergo copyediting, typesetting, and review of the resulting proof before it is published in its final form. Please note that during the production process errors may be discovered which could affect the content, and all legal disclaimers that apply to the journal pertain.

# Comparison of periodic mesh and free mesh on the mechanical properties prediction of 3D braided composites

Chao Zhang<sup>a,\*</sup>, JL Curiel-Sosa<sup>b</sup>, Tinh Quoc Bui<sup>c</sup>

<sup>a</sup>School of Mechanical Engineering, Jiangsu University, Zhenjiang, China

<sup>b</sup>Department of Mechanical Engineering, The University of Sheffield, Sheffield, UK

<sup>c</sup>Department of Civil and Environmental Engineering, Tokyo Institute of Technology, Tokyo, Japan

\*Corresponding author: Chao Zhang, E-mail: zhangchao@ujs.edu.cn, Tel: +86 511 88780169, Fax: +86 511 88790627, Department of Mechanical Design, 301 Xuefu Road, Zhenjiang, 212013, Jiangsu, China

**Abstract:** Periodic unit-cells are the premises for applying the periodic boundary conditions in the meso-scale finite element analysis of textile composites. However, due to the extremely complicated microstructure, there is a conflict between high-quality quick mesh generation and efficient application of periodic boundary conditions. A freely generated mesh of the unit-cell combined with more general periodic boundary conditions is assumed to be a more practical approach. In this paper, the general periodic boundary conditions are imposed by establishing linear constraint equations between master surface nodes and slave surface nodes of the unit-cell on ABAQUS software platform. For the same unit-cell model of 3D braided composites with periodic mesh and free mesh, the deformation, stress distribution and the predicted stiffness and strength properties under typical loadings are compared. The numerical results obtained by means of free mesh unit-cell agree well with those using periodic mesh proving the effectiveness and practicability of the new approach. It can be remarked that the general periodic boundary conditions are suitable for the free mesh generation of unit-cells for a complicated microstructure reducing the difficulty of meshing and improving the quality of mesh generation.

**Key words:** 3D braided composites, unit-cell, periodic boundary conditions, textile composite, mesh generation, finite element analysis

## 1 Introduction

Textile composites are increasingly used in aerospace, automotive, marine and other industries due to their outstanding performances over the conventional laminated composites, including better structural integrity, more balanced properties, higher damage tolerance and lower production costs. However, the microstructure of textile composites is much more complicated than the laminated composites, which brings great difficulties to their mechanical analysis. Fortunately, the microstructure of textile composites shows periodicity. Therefore, the mechanical properties of composite structures are often investigated by a micromechanical method based on a representative unit-cell model, so-called multi-scale techniques. The interested reader can refer to [1-3] for further details on multi-scale techniques. So far, theoretical analysis [4-7] and finite element method [8-15] have been widely employed.

The theoretical analysis is conducted by means of a volume averaging method to attain the overall material properties of the textile composite, including the stiffness averaging method and the compliance averaging method by imposing iso-strain and iso-stress assumptions respectively. Although theoretical analysis is straightforward to implement, it can only obtain the elastic moduli and does not reveal the accurate micro stress distribution and damage characteristics of the textile composites. On the other hand, the Finite Element Method (FEM) overcomes these limitations and it is appropriate for simulating the damage initiation and propagation in the composites. Therefore, besides the study on the stiffness properties [8-11], the strength and damage properties [12-15] of textile composites have been investigated by using meso-scale FEM.

In the finite element analysis based on the unit-cell model, the application of reasonable boundary conditions is an important step to obtain an accurate mechanical response. For continuous materials with periodic microstructure, two continuity conditions need to be satisfied at the boundaries of the neighboring unit-cells at the same time: (1) the displacement should be continuous; (2) the traction should be continuous. For the treatment of the boundary conditions of the unit-cell model of textile composites, homogeneous strain and stress boundary conditions were adopted by some researchers [16-18] to simplify the loading application process. However, it has been proven that [19] if the homogeneous strain boundary conditions are imposed in the unit-cell, the upper-bound of the material elastic constants are obtained while the traction continuity condition cannot be satisfied. Again, if the homogeneous stress boundary conditions are imposed in the unit-cell, the lower-bound of elastic constants are obtained while the displacement continuity condition cannot be satisfied. Whitcomb et al. [20], Xia et al. [21] and Li et al. [22] presented the mathematical expressions of the periodic boundary conditions and applied them to different textile composites. Meso-scale finite element analyses with periodic boundary conditions provide accurate mechanical behavior.

Due to the complicated reinforcement architecture of textile composites, mesh generation may be a large obstacle for meso-scale finite element analysis even with sophisticated meshing tools. The conformal meshing method needs a large number of meshes to coincide with the complex boundaries between the impregnated yarns and the matrix. Meanwhile, many irregular elements appear in these boundaries which result in negative influences on the performance prediction. However, the premise of applying the periodic boundary conditions is to ensure identical mesh at opposite surfaces of the unit-cell, that is, the periodic mesh is required. This further increases the difficulty of the mesh generation and also reduces the quality of the generated mesh. If it is not required to make

any restrictions (so-called free mesh) on the paired surfaces of the unit-cell, the mesh generation becomes relatively easy and the mesh quality can be improved. Accordingly, the more general periodic boundary conditions should be developed.

The present work provides a new insight on the assessment of the effectiveness and practicability of the developed general periodic boundary conditions scheme. Herein, the application of general periodic boundary conditions is performed by imposing multi-point constraint equations to the related nodes on the paired surfaces, edges and corners of the unit-cell model. The mechanical behavior prediction of 3D braided composites, such as the deformation, stress distribution, stiffness, strength properties and damage, under typical loading cases are compared between the unit-cells with periodic mesh and free mesh. The comparison results proved that the general periodic boundary conditions are convenient for free meshing of complex unit-cell configurations and applicable to the meso-scale finite element analysis.

## 2 Periodic boundary conditions and their application

### 2.1 Selection of unit-cell model

The expressions of periodic boundary conditions are associated with the selection of repetitive cell structure. For the periodic structure in Fig. 1(a), the unit-cell is selected as shown in Fig. 1(b). It is the representative volume that can re-create the whole structure only by spatial translation symmetries without using rotation or reflection symmetries. Certainly, if further, using the reflection symmetries, the size of the unit-cell model can be reduced to a quarter (shown in Fig. 1(c)). Whitcomb et al. [20], Carvalho et al. [23] and Li et al. [24, 25] presented different expression forms of the periodic boundary conditions of the repetitive cell according to the specific structural characteristics of the textile composites. In summary, these expressions depend on the structural configuration of the composites, the selection of repetitive cell model and the applied load conditions.

Reducing a unit-cell into a smaller repetitive cell can lessen the number of nodes and elements required which in turn reduce the computation cost. However, the reduction of unit-cell will considerably increase the complexity for applying the periodic boundary conditions. Currently, with the rapid development of computer hardware, the consideration of computational cost associated to the unit-cell model can be neglected unless it is in a very complex nonlinear problem. The substantial increase of complexity of the periodic boundary conditions is the key reason for not reducing a unit-cell into a smaller repetitive cell.

### 2.2 Periodic boundary conditions

The textile composites are considered as periodic structures and composed of periodic arrangement of unit-cells; and the finite element analysis is based on the unit-cell model, therefore, the periodic boundary conditions should be imposed to replicate the repeating nature. Furthermore, the displacement continuity condition and traction continuity condition should be satisfied at the opposite boundaries of the neighboring unit-cells. Therefore, the unified displacement-difference periodic boundary conditions developed by Xia et al. [21], which can guarantee the two continuity conditions [26], are briefly summarized here first.

The displacement field for the periodic structure can be presented as

$$u_i = \bar{\varepsilon}_{ik} x_k + u_i^* \quad (1)$$

In the above equation,  $\bar{\varepsilon}_{ik}$  are the average strains of the unit-cell,  $x_k$  is the Cartesian coordinate of a unit-cell point

and  $u_i^*$  is the periodic part of the displacement components on the boundary surfaces.

Eq. (1) is difficult to be imposed on the unit-cell boundaries because of the unknown periodic part. Fortunately, for most unit-cells, the boundary surfaces always appear in parallel pairs. The displacements on a pair of parallel opposite boundary surfaces can be given as

$$u_i^{j+} = \bar{\varepsilon}_{ik} x_k^{j+} + u_i^* \quad (2)$$

$$u_i^{j-} = \bar{\varepsilon}_{ik} x_k^{j-} + u_i^* \quad (3)$$

where the index  $j+$  means along the positive  $X_j$  direction and  $j-$  means along the negative  $X_j$  direction.

Since  $u_i^*$  is identical on the two parallel boundaries, the difference between the above two equations is

$$u_i^{j+} - u_i^{j-} = \bar{\varepsilon}_{ik} (x_k^{j+} - x_k^{j-}) = \bar{\varepsilon}_{ik} \Delta x_k^j \quad (4)$$

The right side of the above equation becomes constant once  $\bar{\varepsilon}_{ik}$  is specified, since  $\Delta x_k^j$  are constants for each pair of boundary surfaces. Eq. (4) does not contain the periodic part of the displacement components and can be applied easily in the finite element analysis by establishing the linear constraint equations between corresponding nodes.

It deserves mentioning that either force or displacement can be used as the applied load in the finite element analysis. In this paper, the displacement loading mode is employed.

### 2.3 Application of periodic boundary conditions in finite element analysis

In the finite element analysis, the traction boundary conditions are automatically satisfied by the minimum total potential energy principle. This kind of boundary conditions is named as natural boundary conditions. Accordingly, to apply the periodic boundary conditions, only imposing the displacement boundary conditions is sufficient. Of course, the uniqueness and certainty of the numerical results can be guaranteed. The periodic displacement boundary conditions are imposed by establishing the linear constraint equations between the corresponding nodes on the surface of the unit-cell. This is the reason why periodic boundary conditions are also called as equation boundary conditions.

Up to date, in most references, only the mathematical expressions of periodic boundary conditions proposed by Whitcomb et al. [20], Xia et al. [21] and Li et al. [22] are introduced. However, how to implement the periodic boundary conditions in finite element analysis is rarely mentioned. In this section, the constraint equations of periodic boundary conditions between the related nodes on the paired surfaces, edges and corners of the unit-cell model are expressed in detail, which provides certain references to the researchers in the field of micromechanical analysis of textile composites.

#### 2.3.1 Constraint equations between surface nodes

As shown in Fig. 2, the length, width and height of the cuboid unit-cell or representative volume are  $W_x$ ,  $W_y$  and  $h$ , respectively. The origin of the coordinates is point  $D$ . Under the six typical strain loadings  $(\varepsilon_x^0, \varepsilon_y^0, \varepsilon_z^0, \gamma_{xy}^0, \gamma_{xz}^0, \gamma_{yz}^0)$ , the periodic boundary conditions given by Eq. (4) can be realized by the following equations:

On the opposite surfaces perpendicular to the  $x$  axis:

$$\begin{cases} u|_{x=W_x} - u|_{x=0} = W_x \varepsilon_x^0 \\ v|_{x=W_x} - v|_{x=0} = 0 \\ w|_{x=W_x} - w|_{x=0} = 0 \end{cases} \quad (5)$$

On the opposite surfaces perpendicular to the  $y$  axis:

$$\begin{cases} u|_{y=W_y} - u|_{y=0} = W_y \gamma_{xy}^0 \\ v|_{y=W_y} - v|_{y=0} = W_y \varepsilon_y^0 \\ w|_{y=W_y} - w|_{y=0} = 0 \end{cases} \quad (6)$$

On the opposite surfaces perpendicular to the  $z$  axis:

$$\begin{cases} u|_{z=h} - u|_{z=0} = h \gamma_{xz}^0 \\ v|_{z=h} - v|_{z=0} = h \gamma_{yz}^0 \\ w|_{z=h} - w|_{z=0} = h \varepsilon_z^0 \end{cases} \quad (7)$$

In the above equations, three coordinate planes  $x=W_x$ ,  $y=W_y$ ,  $z=h$  are defined as master planes, and the nodes on them are called master nodes; the parallel planes opposite to master planes are defined as slave planes and nodes on them are called slave nodes. For the master surface nodes and slave surface nodes ( $O'-O$ ,  $P'-P$  and  $Q'-Q$  as shown in Fig. 2), the linear constraint equations of periodic boundary conditions have been given by Eqs. (5) - (7).

### 2.3.2 Constraint equations between edge nodes

For the nodes on the edges and corners of the unit-cell model, they located in the intersection planes and lines of the coordinate planes, thus they satisfy two or three groups of Eqs. (5) - (7). However, these equations are not independent to each other. If all these constraint equations are applied in the finite element analysis, the unit-cell model will be over constrained and the computation cannot be carried out. Therefore, the constraint equations of the corresponding nodes on the edges and corners should be combined to form the independent equations.

For the 12 edges of the unit-cell model, they can be divided into three types: parallel to the  $x$  axis ( $AD$ ,  $BC$ ,  $FG$  and  $EH$ ), parallel to the  $y$  axis ( $CD$ ,  $BA$ ,  $FE$  and  $GH$ ) and parallel to the  $z$  axis ( $HD$ ,  $EA$ ,  $FB$  and  $GC$ ). In this paper, we only give three groups of linear constraint equations between the four edges that are parallel to  $z$  axis when the  $HD$  edge is defined as the reference edge, namely

$$\begin{cases} u_{EA} - u_{HD} = W_x \varepsilon_x^0 \\ v_{EA} - v_{HD} = 0 \\ w_{EA} - w_{HD} = 0 \end{cases} \quad (8)$$

$$\begin{cases} u_{FB} - u_{HD} = W_x \varepsilon_x^0 + W_y \gamma_{xy}^0 \\ v_{FB} - v_{HD} = W_y \varepsilon_y^0 \\ w_{FB} - w_{HD} = 0 \end{cases} \quad (9)$$

$$\begin{cases} u_{GC} - u_{HD} = W_y \gamma_{xy}^0 \\ v_{GC} - v_{HD} = W_y \varepsilon_y^0 \\ w_{GC} - w_{HD} = 0 \end{cases} \quad (10)$$

Applying the above constraint equations can ensure the complete constraint of these four edges. That is, the under constraint and over constraint problems will not appear in the subsequent calculation. For the other two types of edge constraint equations, referred to Eqs. (8) - (10) and combined with the deformation states of the unit-cell under corresponding strain loadings, they can be easily derived.

### 2.3.3 Constraint equations between corner nodes

Special attention should be paid to the constraint equations between 8 corner nodes of the unit-cell model. Selecting node  $D$  as the reference point, the constraint equations between nodes  $E, F, G$  and  $D$  are given as:

$$\begin{cases} u_E - u_D = W_x \varepsilon_x^0 + h\gamma_{xz}^0 \\ v_E - v_D = h\gamma_{yz}^0 \\ w_E - w_D = h\varepsilon_z^0 \end{cases} \quad (11)$$

$$\begin{cases} u_F - u_D = W_x \varepsilon_x^0 + W_y \gamma_{xy}^0 + h\gamma_{xz}^0 \\ v_F - v_D = W_y \varepsilon_y^0 + h\gamma_{yz}^0 \\ w_F - w_D = h\varepsilon_z^0 \end{cases} \quad (12)$$

$$\begin{cases} u_G - u_D = W_y \gamma_{xy}^0 + h\gamma_{xz}^0 \\ v_G - v_D = W_y \varepsilon_y^0 + h\gamma_{yz}^0 \\ w_G - w_D = h\varepsilon_z^0 \end{cases} \quad (13)$$

Similarly, for the constraint equations between other corner nodes  $A, B, C, H$  and the reference point  $D$ , referred to Eqs. (11) - (13) and combined with the corresponding deformation states, they can also be easily achieved.

## 3 General Periodic boundary conditions and their application

It should be noted that imposing the above periodic boundary conditions to the unit-cell is dependent on a perfect periodic mesh. However, perfect periodic mesh may increase the difficulty of meshing a unit-cell with complex microstructure and reduce the quality of the generated mesh. Free mesh (non-periodic) is regard as a more practical approach. To the unit-cell model with free mesh generation, Nguyen et al. [27] and Jarvis and Garnich [28] developed the concept of general periodic boundary conditions. In the present paper, the general periodic boundary conditions scheme will be implemented explicitly in the meso-scale finite element analysis on the platform of ABAQUS software, and the effectiveness and applicability will be verified by comparison research.

### 3.1 General periodic boundary conditions

Due to the non-periodic meshing, the mapping point  $M$  of a master node  $M'$  on the slave plane is not just in the position of a node but within an element. The displacement of the point  $M$  can be determined by nodal displacement interpolation, namely

$$\{u\} = [N]\{\delta\} \quad (14)$$

where  $\{u\}$  is the displacement matrix of the mapping point,  $[N]$  is the shape function matrix of the element, and  $\{\delta\}$  is the displacement matrix of the element nodes.

Owing to the complexity of the microstructure, 3D solid tetrahedral elements (C3D4) available in ABAQUS are always adopted for mesh generation of textile composites because of its excellent geometry adaptability. In this paper, C3D4 elements are used for the periodic mesh and the free mesh generation of 3D braided composites. At this time, the mapping point  $M$  is surrounded by a triangular element on the slave plane, as shown in Fig. 2. Similar to Eq. (4), the general periodic boundary conditions can be written as [28]

$$u_i^{j+}(M) - [N_1(M) \ N_2(M) \ N_3(M)] \begin{bmatrix} u_i^{j-}(S_1) \\ u_i^{j-}(S_2) \\ u_i^{j-}(S_3) \end{bmatrix} = \bar{\varepsilon}_{ik} \Delta x_k^j \quad (i, j = 1, 2, 3) \quad (15)$$

### 3.2 Application of general periodic boundary conditions in finite element analysis

As shown in Fig. 3, the position of the mapping point  $M$  in  $\Delta S_1 S_2 S_3$  on the slave surface can be given by

$$M = S_1 + x*(S_2 - S_1) + y*(S_3 - S_1) \quad (16)$$

If the coefficient  $x$  and  $y$  satisfy Eq. (17), it can be confirmed that the mapping point  $M$  is located in the triangular element (including the boundary).

$$x \geq 0, y \geq 0, x + y \leq 1 \quad (17)$$

Moreover, the shape function matrix  $[N]$  of the element can be determined by the coordinates of point  $M$  and vertices of  $\Delta S_1 S_2 S_3$ .

For the application of general periodic boundary conditions, to realize the constraint equation between the surface nodes, it is just needed to replace the second term in Eqs. (5) - (7) with Eq. (14). For the edges of the unit-cell, the mapping points of the edge nodes locate between two nodes of the reference edge. At this time, the shape function matrix  $[N]$  is similar to that of one-dimensional bar element. It is also just needed to replace the second term in Eqs. (8) - (10) with Eq. (14). For the corners of the unit-cell, the constraint equations between the corner nodes are identical to Eqs. (11) - (13). In particular, when the element shape function matrix  $[N]$  is only one component of 1 while the rest of 0 (i.e. periodic meshing), Eq. (15) exactly reduces to the Eq. (4) as periodic boundary conditions.

Finally, a FORTRAN pre-compiler code involving these constraint equations is written and implemented based on the platform of finite element software ABAQUS.

## 4 Finite element model

### 4.1 Unit-cell structural model

In order to verify the effectiveness and applicability of the explicit general periodic boundary conditions given in this paper, a unit-cell structural model of 3D braided composites proposed by Xu and Xu [29] is utilized here for comparison analysis. The cross section shape of the braiding yarns is considered as octagon containing an inscribed ellipse. The relationship between the major radius  $a$  and minor radius  $b$  of the ellipse and interior braiding angle of braided composites  $\gamma$ , is expressed as

$$a = \sqrt{3}b \cos \gamma \quad (18)$$

As displayed in Fig. 4,  $W_x$ ,  $W_y$  and  $h$  represent the width, thickness and height of the unit-cell model respectively, and they can be calculated as:

$$W_x = 4\sqrt{2}b \quad (19)$$

$$W_y = 4\sqrt{2}b \quad (20)$$

$$h = 8b / \tan \gamma \quad (21)$$

The unit-cell model of 3D braided composites consists of braiding yarns and resin matrix. The braiding yarn containing thousands of fibers and matrix is considered as transversely isotropic unidirectional composites in local coordinate and the resin matrix is assumed to be isotropic. For the local coordinate definition of braiding yarn in a specify orientation, local 1-axis follows the yarn centerline and local 3-axis is in the upright plane perpendicular to the  $x$ - $y$  plane of the global coordinate, as shown in Fig. 4. The Stiffness and strength properties of constituents are listed in Table 1, and the structural parameters of the unit-cell model in this paper are given as follows:  $\gamma=46.4$ ,  $W_x=W_y=1.662\text{mm}$ ,  $h=2.238\text{mm}$ ,  $V_f=52\%$ .

## 4.2 Finite element meshing

Attributable to the complexity of the microstructure, the solid tetrahedral elements (C3D4) are utilized to mesh the unit-cell model of 3D braided composites. The merged coincident meshes are adopted on the interfaces, to be precise, the interfaces between the yarns and matrix are assumed to be perfectly bonded. Specifically, for periodic meshing, the number and the position of the nodes on the master and slave planes must be exactly the same, which is accomplished by surface mesh replication method. However, for free meshing, no restriction is placed on the paired planes of the unit-cell and high-quality mesh is easier to generate. The unit-cell model with periodic mesh is composed of 7, 992 nodes and 40,452 C3D4 elements, and the unit-cell model with free mesh consists of 6, 923 nodes and 33, 515 C3D4 elements respectively, as shown in Fig. 5.

## 4.3 Prediction of effective elastic properties

In this paper, homogenization method is utilized in order to predict the mechanical properties of textile composites. That is, the heterogeneous composites in the micro-scale are considered a homogeneous material in the macro-scale. The stress-strain relationship of a unit-cell can be computed by

$$\bar{\sigma} = C\bar{\epsilon} \quad (22)$$

where  $C$  is the effective stiffness matrix.  $\bar{\sigma}$  and  $\bar{\epsilon}$  are the global average stress and global average strain defined by

$$\bar{\sigma}_{ij} = \frac{1}{V} \int_V \sigma_{ij} dV \quad \bar{\epsilon}_{ij} = \frac{1}{V} \int_V \epsilon_{ij} dV \quad (i, j=1, 2, 3) \quad (23)$$

In the cuboid unit-cell,  $\bar{\epsilon}_{ij}$  is known in advance when applying periodic displacement boundary conditions. For  $\bar{\sigma}_{ij}$ , one has

$$\bar{\sigma}_{ij} = \frac{(P_i)_j}{S_j} \quad (i, j=1, 2, 3) \quad (24)$$

In the above equation,  $(P_i)_j$  is the  $i$ th resultant forces on the  $j$ th boundary surface and  $S_j$  is the area of the  $j$ th boundary surface.

The elastic constants of the unit-cell can be calculated by

$$E_i = \frac{\bar{\sigma}_i}{\bar{\epsilon}_i}, \quad \mu_{ij} = -\frac{\bar{\epsilon}_i}{\bar{\epsilon}_j}, \quad G_{ij} = \frac{\bar{\sigma}_{ij}}{\bar{\epsilon}_{ij}} \quad (i, j=1, 2, 3) \quad (25)$$

#### 4.4 Prediction of damage and strength properties

Physical experiments are expensive, time-consuming, and confined to certain structural parameters. Moreover, it is difficult to identify the damage modes and investigate the damage evolution process of the interior components. The damage simulation by finite element method can conduct virtual tests of the composites and provide insights into the local responses thus can overcome the limitations in physical experiments.

Damage initiation and damage evolution can be simulated by damage mechanism, which consist of failure criteria and material degradation. In this paper, 3D Hashin failure criteria [30] are applied to define the damage initiation of braiding yarns. In Hashin criteria, four distinct failure modes are considered: yarn tensile failure in  $L$  direction, yarn compressive failure in  $L$  direction, yarn tensile and shear failure in  $T$  and  $Z$  direction, and yarn compressive and shear failure in  $T$  and  $Z$  direction. Herein,  $L$ - $T$ - $Z$  rectangular coordinate is local coordinate definition of braiding yarn, and  $L$  axis,  $T$  axis and  $Z$  axis indicate the axial and two transverse directions. Maximum stress criteria are employed to define the initiation of matrix cracking.

Once the damage initiation criteria are satisfied, further loading will cause degradation of material stiffness constants. The reduction of the stiffness constants is controlled by damage variables ranged from 0 (initial undamaged) to 1 (completely damaged) according to the damage situation. In this paper, a gradual degradation scheme coupling with Murakami damage model proposed by Lapczyk et al. [31] and Fang et al. [13] is used to characterize the damage process of the yarns and matrix. More detailed analysis about the damage model of 3D braided composites can be found in reference [13].

Finally, A user material subroutine (UMAT) involving the damage model is developed and implemented in the finite element software ABAQUS. The whole process of damage evolution of 3D braided composites is simulated, and the damage mechanisms are revealed in the simulation process. The strength properties of 3D braided composites are predicted from the computed stress-strain curves. The approach presented herein is suitable for inclusion of advanced damage models integrating initiation and evolution [32, 33] although these have not been attempted at this time.

## 5 Results and discussions

### 5.1 Preliminary validation of the application

To validate the boundary conditions derived based on the unit-cell model, a simple method proposed by Li et al. [24] is implemented first. A small case of homogeneous isotropic block is selected as a unit-cell and the general

periodic boundary conditions are imposed. Under six typical loading conditions ( $\epsilon_x^0, \epsilon_y^0, \epsilon_z^0, \gamma_{xy}^0, \gamma_{xz}^0, \gamma_{yz}^0$ ), perfectly uniform stress and strain fields can be obtained. The stresses and strains are same to the average stresses and strains predicted by material properties assigned to the unit-cell model, which preliminarily verifies the applied boundary conditions. By this approach, most human mistakes in applying complicated boundary conditions can be avoided.

## 5.2 Comparison of elastic properties

Due to the spatial rotation characteristics of 3D braided composites, the deformation and stress distribution of the unit-cell model under  $x$  and  $y$  tension, as well as under  $xz$  and  $yz$  shear, are similar. Accordingly, only the comparison results of elastic properties under  $x$  tension,  $z$  tension,  $xy$  shear and  $xz$  shear are given here.

Fig. 6 displays the comparison of deformation between unit-cell models with periodic mesh and free mesh (the deformation scale factor is 35). It can be found that the deformation stations of the periodic meshing unit-cell are consistent with that of free meshing under all the four typical loading cases. The boundary surfaces of the unit-cell are no longer maintained as planes but warped. Especially, in the  $z$  tension, the warping extent on the top and bottom surface is most obvious but weaker on the other two paired surfaces. This is mainly attributed to the fact that the unit-cell model does not have the symmetries of geometrical structure and physical properties. However, the parallel opposite boundary surfaces have the same deformation, which can guarantee the displacement continuity between the neighboring unit-cells and provide a reasonable stress distribution. It can also be seen that the four deformation stations shown in Fig. 6 correctly reflect the corresponding load characteristics of the applied boundary conditions.

Fig. 7 demonstrates the comparison of von-Mises stress distributions between unit-cell models with periodic and free mesh on un-deformed shape. The paired opposite surfaces totally have the same stress distribution, which ensures the traction continuity condition at the opposite boundary surfaces of the unit-cell models. Note that the stress in the braiding yarns is obviously larger than that in the matrix and the braiding yarns bear main loads under all the loading cases. This is because the stiffness of braiding yarn is much larger than matrix and the load distribution is determined by the stiffness properties. However, under different loadings, the load bearing mechanism of braiding yarn is different thus the mechanical response characteristics of the unit-cell model are also different. It can also be observed that the stress distributions of the two unit-cell models are very close to each other when subjected to the same loading conditions. That is, the stress and strain fields of the unit-cell model with general periodic boundary conditions agree well with that under periodic boundary conditions.

Next, the quantitative comparison results of the unit-cell model with two different meshes are mainly presented by the following stiffness and strength predictions. Table 2 displays the predicted elastic constants of the unit-cell model with periodic mesh and free mesh. From Table 2, it is seen that the unit-cell model is almost perfect transversely isotropic and the corresponding prediction results are in good agreement in these two cases. It has been proved that excellent elastic prediction results can be obtained compared with the numerical simulation data based on the unit-cell model imposed by periodic boundary conditions [8-11]. Consequently, the results in Table 2 further verify the effectiveness and validity of the general periodic boundary conditions in the application of elastic properties prediction by unit-cell model with free mesh.

## 5.3 Comparison of strength and damage properties

### 5.3.1 Stress-strain curves

Fig. 8 illustrates the computed stress-strain curves of unit-cell models with periodic mesh and free mesh. Similarly, only the comparison results under  $x$  tension,  $z$  tension,  $xy$  shear and  $xz$  shear are given. In Fig. 8, PM refers to periodic mesh and FM refers to free mesh. It is obvious that the computed stress-strain curves of the

periodic meshing unit-cell agree well with that of free meshing under the same loading cases. Actually, the carbon-fiber reinforced 3D braided composites tends to exhibit brittle breaking characteristics in experiment and the composites will fracture when the experimental stress-strain curve reaching the maximum stress. However, the computed stress-strain curves provide the whole simulation process from damage initiation, propagation to catastrophic failure. After reaching the maximum stress, the computed curves decrease rapidly or gradually according to the loading cases and then the materials loss the carrying capacity. The extended unloading observed in the computed stress-strain curves is considered as a numerical artifact because the experimental specimens most likely have a more brittle fiber failure, whereas the computed curves have a more gradual unloading to promote the numerical stability [15]. The comparison results of predicted strength parameters and failure strains are summarized in Table 3. Obviously, these predicted results are very close, thus verifies that the general periodic boundary conditions are also suitable for strength properties prediction by unit-cell model with free mesh.

### 5.3.2 Failure mode and damage mechanism

The advantage of the meso-scale finite element method is not only the global stiffness and strength properties of the composites but also various failure mode and damage mechanism, can be studied through the analysis [21]. In this paper, the damage evolution processes of unit-cell models with periodic mesh and free mesh under typical loads are simulated. The failure mode and damage mechanism are different under different loading cases. It is found that the main failure modes of the braided composites are yarn tensile and shear failure in  $T$  and  $Z$  direction and matrix tension cracking under  $x$  tension load. Yarn compressive and shear failure in  $T$  and  $Z$  direction are very limited and yarn tension and compressive failure in  $L$  direction are not existed. Under  $z$  tension load, the main failure modes are yarn  $T$  compressive and shear failure and matrix cracking.  $L$  tensile fracture occurs in some elements in the braiding yarn, but the quantity is relatively small. Under  $xy$  and  $xz$  shear loads, the main failure modes are yarn  $T$  tension and shear failure, meanwhile,  $L$  compressive fracture occurs in some elements in the braiding yarn and the quantity is relatively large. Fig. 9 depicts the comparison of certain modes damage nephograms between unit-cell models with periodic mesh and free mesh in yarns and matrix under the same strain cases. It can be found that the damage stations always similar in the two mesh status under corresponding loads. Therefore, the general periodic boundary conditions can also be utilized for damage simulation and damage mechanism analysis by unit-cell model with free mesh.

## 6 Conclusions

In this paper, a study is conducted by comparing the periodic mesh and the free mesh on the mechanical properties prediction of 3D braided composites. For the unit-cell model with free mesh generation, the more general periodic boundary conditions are applied by establishing the multi-point constraint equations between the related nodes on the paired surfaces, edges and corners of the unit-cell model. To verify the effectiveness and validity of the general periodic boundary conditions, the deformation, stress distribution and the predicted stiffness and strength properties of the unit-cell model of 3D braided composites with periodic mesh and free mesh are compared. Some conclusions can be drawn herein.

(1) In the finite element analysis, the edge nodes and corner nodes of the unit-cell model meet two or three groups of constraint equations for surface nodes simultaneously. However, these equations are not independent to each other. Before applying the periodic boundary conditions, the constraint equations of the nodes at these positions should be merged into independent equations.

(2) Under non-periodic meshing condition, the mapping point of a master node on the slave plane is not just in the position of a node but within an element. When establishing the linear constraint equation, the displacement of the mapping point can be obtained by interpolating the nodal displacement of the element which surrounds the

mapping point.

(3) Imposing the general periodic boundary conditions to the free meshing unit-cell model, realistic strain and stress fields as well as reasonable stiffness and strength properties can be obtained. It is proved that the general periodic boundary conditions are suitable for the free mesh of complicated microstructure model and thus can reduce the difficulty of meshing and improve the quality of mesh generation. Therefore, it should be a robust and effective approach in future meso-scale finite element analysis of textile composites.

## Acknowledgements

This work was supported by Postdoctoral Science Foundation of Jiangsu Province (1402101C), Senior Talent Start-up Foundation of Jiangsu University (14JDG136) and Jiangsu Government Scholarship for Overseas Studies.

## References

- [1] Carneiro Molina AJ, Curiel-Sosa JL. A multiscale finite element technique for nonlinear multi-phase materials. *Finite Elem in Anal Des* 2015; 94(C): 64-80.
- [2] Carneiro Molina AJ, Curiel-Sosa JL. A large strains finite element multiscale approach. *Int J Comput Meth Eng Sci Mech* 2016; 17(1): 46-58.
- [3] Mahmood A, Wang X, Zhou C. Modeling strategies of 3D woven composites: A review. *Compos Struct* 2011; 93: 1947-1963.
- [4] Sun HY, Qiao X. Prediction of mechanical properties of three-dimensionally braided composites. *Compos Sci Technol* 1997; 57(6): 623-629.
- [5] Byun JH. The analytical characterization of 2-D braided textile composites. *Compos Sci Technol* 2000; 60(5): 705-716.
- [6] Shokrieh M, Mazloomi M. A new analytical model for calculation of stiffness of three-dimensional four directional braided composites. *Compos Struct* 2012; 94(3): 1005-1015.
- [7] Xu K, Qian XM. A new analytical model on predicting the elastic properties of 3D full five-directional braided composites based on a multiunit cell model. *Compos Part B* 2015; 83: 242-252.
- [8] Wang XF, Wang XW, Zhou GM, Zhou CW. Multi-scale analyses of 3D woven composite based on periodicity boundary conditions. *J Compos Mater* 2007; 41(14): 1773-1788.
- [9] Fang GD, Liang J, Wang Y, Wang BL. The effect of yarn distortion on the mechanical properties of 3D four-directional braided composites. *Compos Part A* 2009; 40(4): 343-350.
- [10] Li DS, Fang DN, Jiang N, Yao XF. Finite element modeling of mechanical properties of 3D five-directional rectangular braided composites. *Compos Part B* 2011; 42(6): 1373-1385.
- [11] Zhang C, Xu XW. Finite element analysis of 3D braided composites based on three unit-cell models. *Compos Struct* 2013; 98: 130-142.
- [12] Miravete A, Bielsa JM, Chiminelli A et al. 3D mesomechanical analysis of three-axial braided composite materials. *Compos Sci Technol* 2006; 66: 2954-2964.
- [13] Fang GD, Liang J, Wang BL. Progressive damage and nonlinear analysis of 3D four-directional braided composites under unidirectional tension. *Compos Struct* 2009; 89: 126-133.
- [14] Lu ZX, Xia B, Yang ZY. Investigation on the tensile properties of three dimensional full five directional braided composites. *Comput Mater Sci* 2013; 77: 445-455.
- [15] Zhang C, Li N, Wang WZ, Binienda WK, Fang HB. Progressive damage simulation of triaxially braided composite using a 3D meso-scale finite element model. *Compos Struct* 2015; 125: 104-116.

- [16] Peng X, Cao J. A dual homogenisation and finite element approach for material characterization of textile composites. *Compos Part B* 2002; 33(1): 45-56.
- [17] Li JC, Chen L, Zhang YF, Pan N. Microstructure and finite element analysis of 3D five directional braided composites. *J Reinf Plast Comp* 2011; 31(2): 107-115.
- [18] Wang C, Zhong YC, Adaikalaraj PF, et al. Strength prediction for bi-axial braided composites by a multi-scale modelling approach. *J Mater Sci* 2016; 51: 6002-6018.
- [19] Hori M, Nemat-Nasser S. On two micromechanics theories for determining micro-macro relations in heterogeneous solids. *Mech Mater* 1999; 31(10): 667-682.
- [20] Whitcomb JD, Chapman CD, Tang XD. Derivation of boundary conditions for micromechanics analysis of plain and satin weave composites. *J Compos Mater* 2000; 34(9): 724-747.
- [21] Xia ZH, Zhang YF, Ellyin F. A unified periodical boundary conditions for representative volume elements of composites and applications. *Int J Solids Struct* 2003; 40(8): 1907-1921.
- [22] Li SG. Boundary conditions for unit cells from periodic microstructures and their implications. *Compos Sci Technol* 2008; 68(9): 1962-1974.
- [23] Carvalho N, Pinho S, Robinson P. Reducing the domain in the mechanical analysis of periodic structures with application to woven composites. *Compos Sci Technol* 2011; 71(7): 969-979.
- [24] Li S, Zhou C, Yu H, Li L. Formulation of a unit cell of a reduced size for plain weave textile composites. *Comput Mater Sci* 2011; 50(5): 1770-1780.
- [25] Li S, Zou Z. The use of central reflection in the formulation of unit cells for micromechanical FEA. *Mech Mater* 2011; 43(12): 824-834.
- [26] Xia Z H, Zhou C W, Yong Q L, Wang XW. On selection of repeated unit cell model and application of unified periodic boundary conditions in micro-mechanical analysis of composites. *Int J Solids Struct* 2006; 43(2): 266-278.
- [27] Nguyen V D, Béchet E, Geuzaine C, Noels L. Imposing periodic boundary condition on arbitrary meshes by polynomial interpolation. *Comput Mater Sci* 2012; 55: 390-406.
- [28] Jarvis A S, Garnich M R. Meso-scale and multicontinuum modeling of a triaxial braided textile composite. *J Compos Mater* 2012; 47(3): 303-314.
- [29] Xu K, Xu XW. On the microstructure model of four-step 3D rectangular braided composites. *Acta Mater Compos Sin* 2006; 23(5): 154-160.
- [30] Hashin Z. Failure criteria for unidirectional fiber composite. *J Appl Mech* 1980; 47: 329-334.
- [31] Lapczyk I, Hurtado JA. Progressive damage modeling in fiber reinforced materials. *Compos Part A* 2007; 38(11): 2333-2341.
- [32] Curiel Sosa JL, Petrinic N, Weigand J. A three-dimensional progressive damage model for fibre-composite materials. *Mech Res Commun* 2008; 35 (4): 219-221.
- [33] Curiel Sosa JL, Phaneendra S, Muñoz JJ. Modeling of mixed damage on fibre-reinforced composite laminates subjected to low velocity impact. *Int J of Damage Mech* 2013; 22(3): 356-374.

## List of Figure Captions

Fig. 1 The selection of unit-cell model

Fig. 2 Equation boundary conditions

Fig. 3 Position relationship between mapping point and triangle element

Fig. 4 Unit-cell structural model of 3D braided composites (a) 3D model of unit-cell (b) Topological relationship of braiding yarns

Fig. 5 Finite element mesh of the unit-cell (a) Periodic mesh (b) Free mesh

Fig. 6 Comparison of deformation between unit-cell models with periodic mesh and free mesh (a)  $x$  tension (b)  $z$  tension (c)  $xy$  shear (d)  $xz$  shear

Fig. 7 Comparison of stress distributions between unit-cell models with periodic mesh and free mesh (a)  $x$  tension (b)  $z$  tension (c)  $xy$  shear (d)  $xz$  shear

Fig. 8 The computed stress-strain curves of unit-cell models with periodic mesh and free mesh

Fig. 9 Comparison of certain modes damage nephograms between unit-cell models with periodic mesh and free mesh

## List of Table Titles

Table 1 Stiffness and strength properties of constituents

Table 2 Predicted elastic constants of unit-cells with periodic mesh and free mesh

Table 3 Predicted strength parameters and failure strains of unit-cells with periodic mesh and free mesh

ACCEPTED MANUSCRIPT

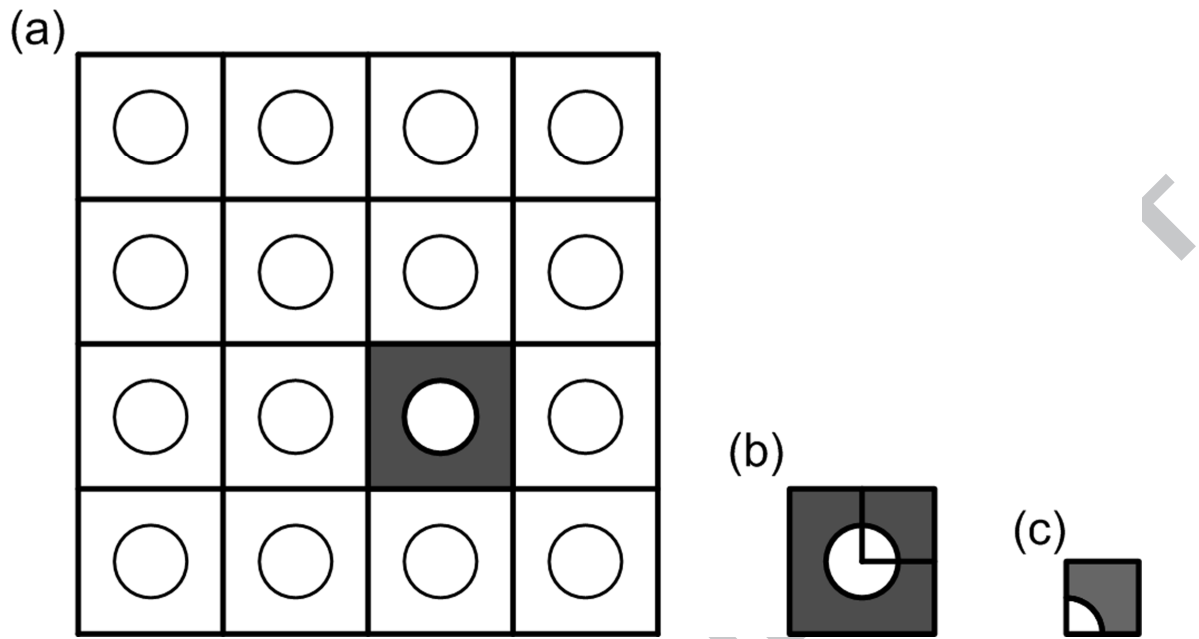


Fig. 1

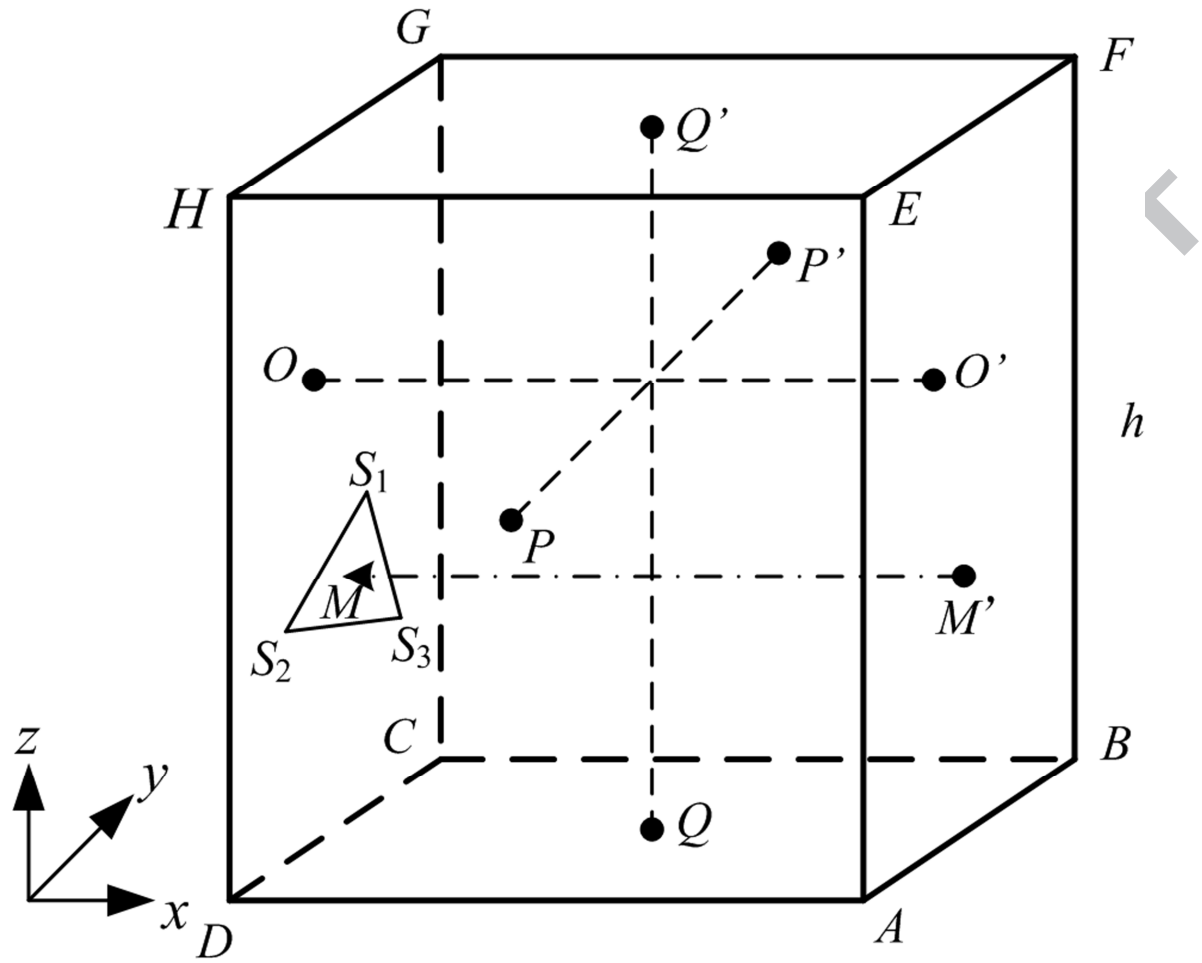


Fig. 2

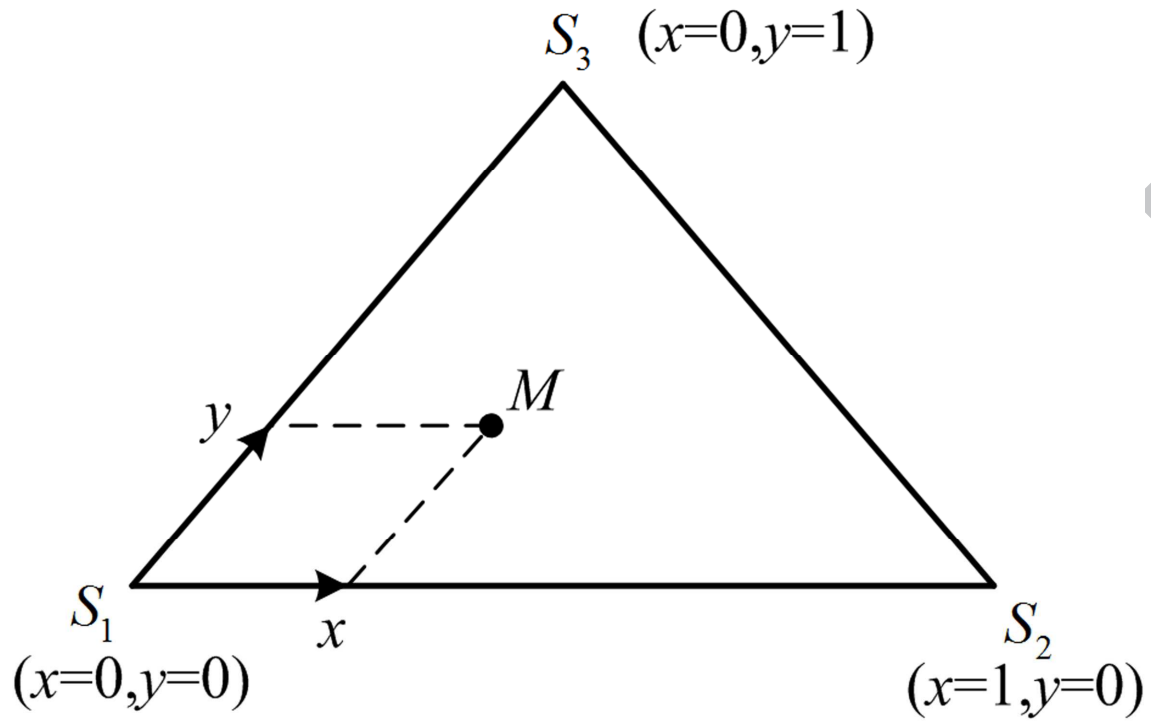


Fig. 3

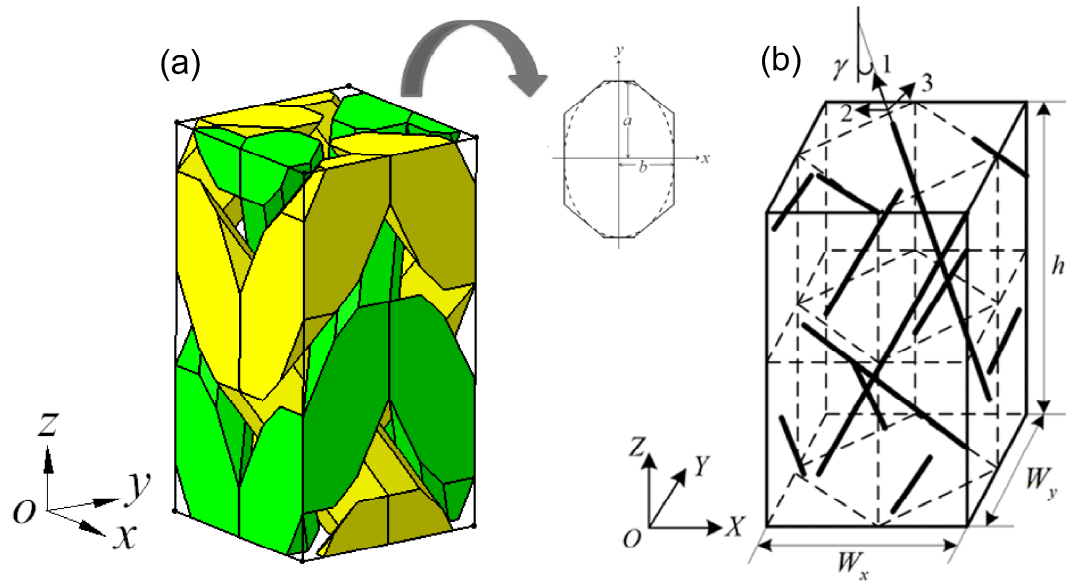


Fig. 4

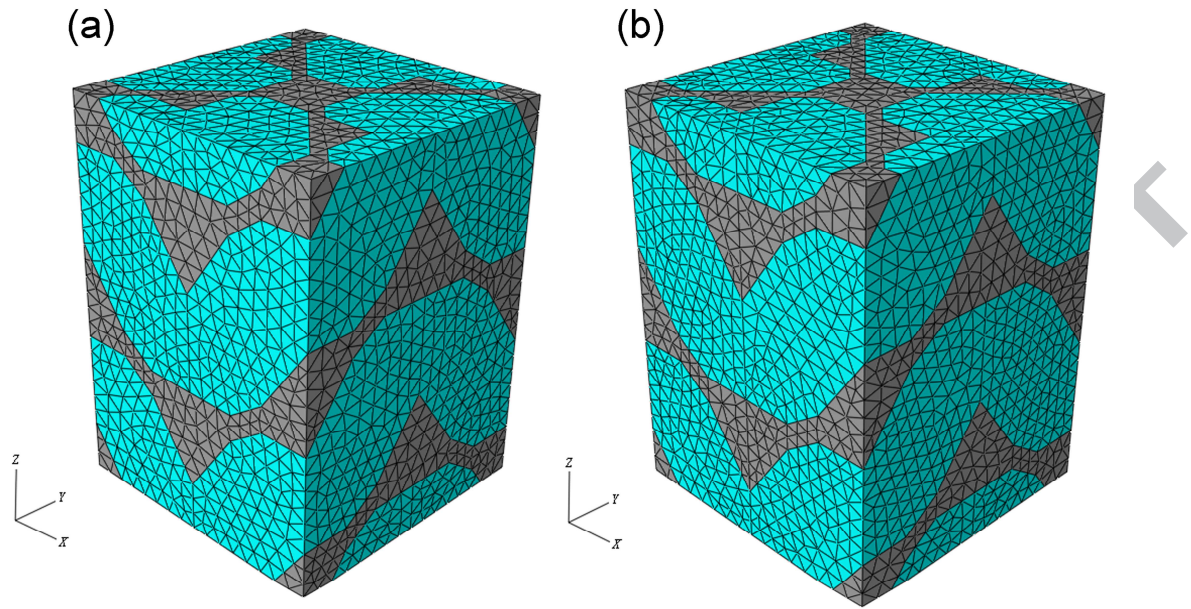


Fig. 5

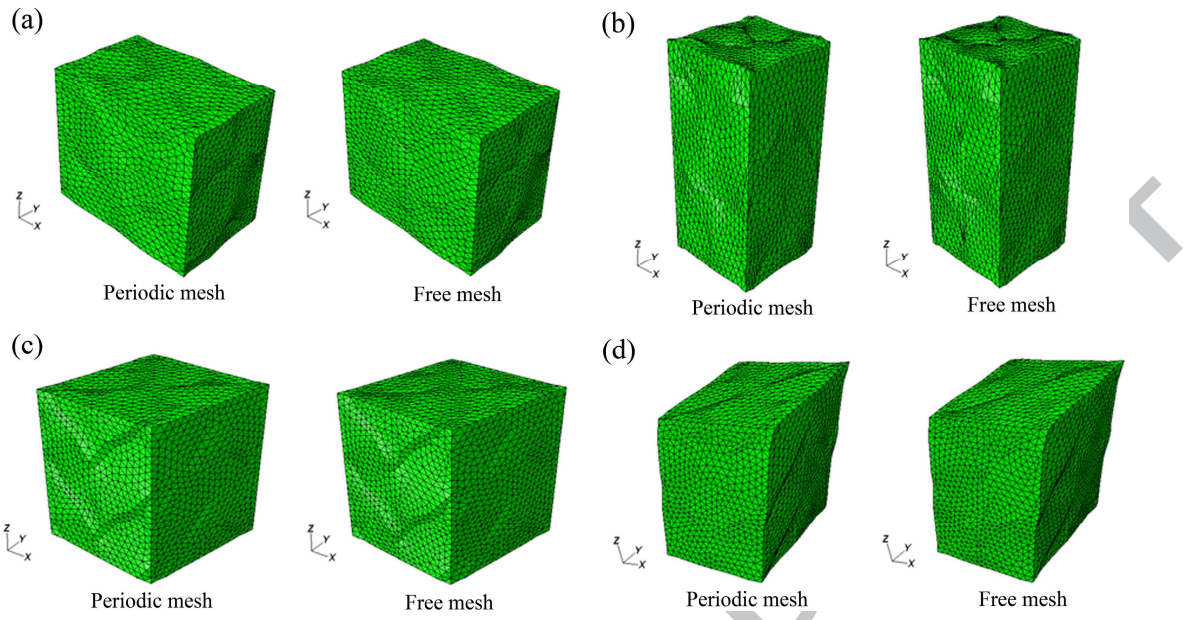


Fig. 6

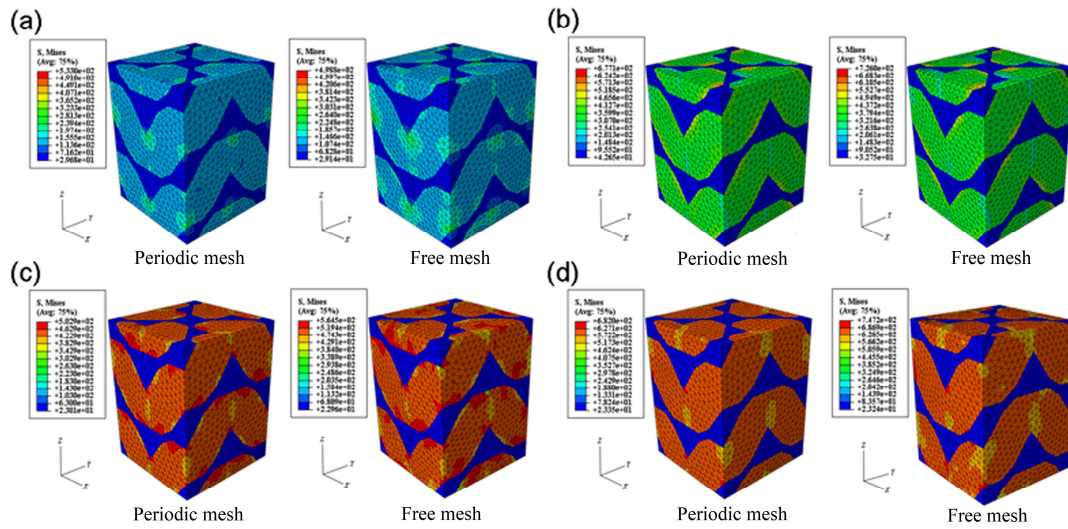


Fig. 7

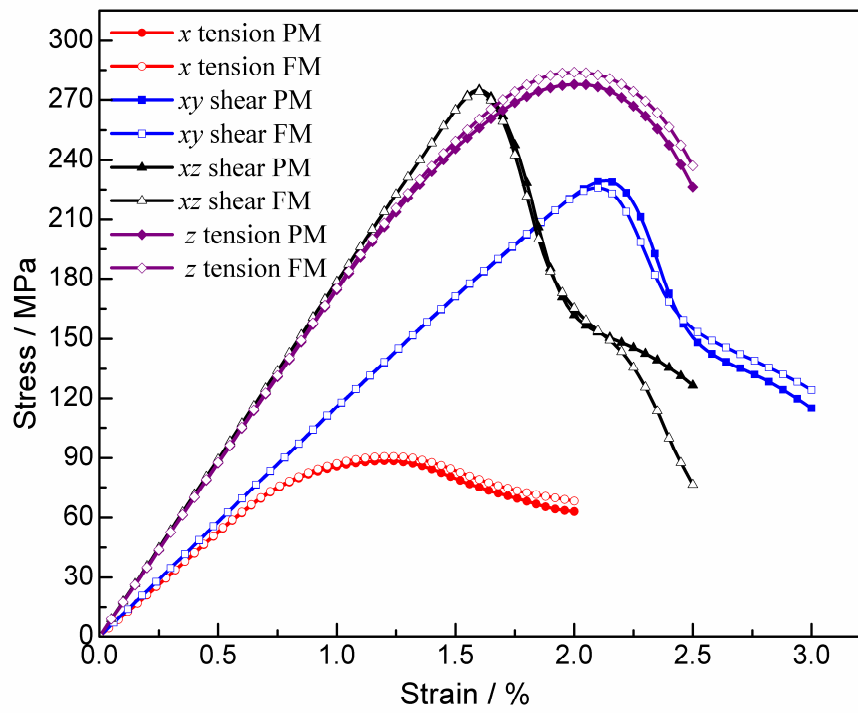


Fig. 8

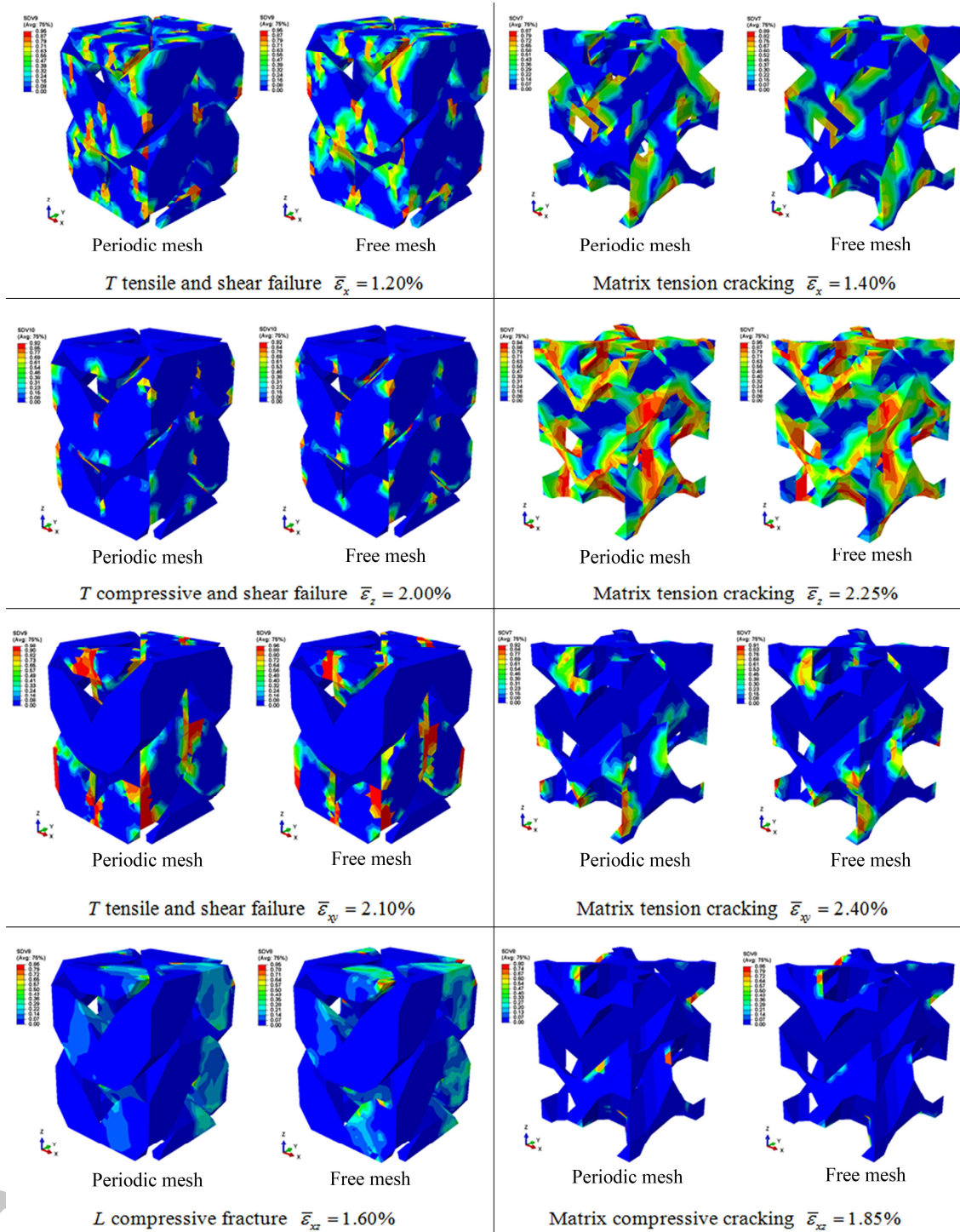


Fig. 9

Table 1 Stiffness and strength properties of constituents

	$E_{f1}$ (GPa)	$E_{f2}$ (GPa)	$G_{f12}$ (GPa)	$G_{f23}$ (GPa)	$\mu_{f12}$	$E_m$ (GPa)	$\mu_m$	$X_T$ (MPa)	$X_C$ (MPa)	$S$ (MPa)
T300	230	40	24	14.3	0.26			3528	2470	
Matrix						3.5	0.35	80	241	100

Table 2 Predicted elastic constants of unit-cells with periodic mesh and free mesh

Elastic constants / Gpa	Periodic mesh	Free mesh
$E_x$	10.55	10.62
$E_y$	10.55	10.61
$E_z$	17.42	17.50
$G_{xz}$	17.80	17.80
$G_{yz}$	17.80	17.79
$G_{xy}$	11.52	11.54
$\mu_{xy}$	0.30	0.30
$\mu_{zx}$	0.56	0.56
$\mu_{zy}$	0.56	0.56

Table 3 Predicted strength parameters and failure strains of unit-cells with periodic mesh and free mesh

	Strength / MPa		Failure strain / %		
	Periodic mesh	Free mesh	Periodic mesh	Free mesh	
$S_x$	88.50	90.77	$\epsilon_x$	1.20	1.24
$S_y$	88.59	91.41	$\epsilon_y$	1.20	1.24
$S_z$	277.75	283.87	$\epsilon_z$	2.00	2.00
$S_{xz}$	275.16	274.14	$\gamma_{xz}$	1.60	1.60
$S_{yz}$	275.03	273.77	$\gamma_{yz}$	1.60	1.60
$S_{xy}$	228.99	225.91	$\gamma_{xy}$	2.10	2.10